

# White Matter Hyperintensities Segmentation In a Few Seconds Using Fully Convolutional Network and Transfer Learning

Yongchao Xu<sup>1,2,3</sup>, Thierry Géraud<sup>1</sup>, Élodie Puybureau<sup>1</sup>,  
Isabelle Bloch<sup>2</sup>, and Joseph Chazalon<sup>1,4</sup>

<sup>1</sup> EPITA Research and Development Laboratory (LRDE)  
Le Kremlin-Bicêtre, France  
`thierry.geraud@lrde.epita.fr`

<sup>2</sup> LTCI, Télécom ParisTech, Université Paris-Saclay, Palaiseau, France

<sup>3</sup> Huazhong University of Science and Technology, Wuhan, China

<sup>4</sup> Université de La Rochelle, La Rochelle, France

**Abstract.** In this paper, we propose a fast automatic method that segments white matter hyperintensities (WMH) in 3D brain MR images, using a fully convolutional network (FCN) and transfer learning. This FCN is the Visual Geometry Group neural network (VGG for short) pre-trained on ImageNet for natural image classification, and fine tuned with the training dataset of the MICCAI WMH Challenge. We consider three images for each slice of the volume to segment: the T1 slice, the FLAIR slice, and the result of a morphological operator that emphasizes small bright structures. These three 2D images are assembled to form a 2D color image, that inputs the FCN to obtain the 2D segmentation of the corresponding slice. We process all slices, and stack the results to form the 3D output segmentation. With such a technique, the segmentation of WMH on a 3D brain volume takes about 10 seconds including pre-processing. Our technique was ranked 6-th over 20 participants at the MICCAI WMH Challenge.

**Keywords:** 3D brain MRI · lesion segmentation · white matter hyperintensities · mathematical morphology · fully convolutional network.

## 1 Introduction

### 1.1 Context

This work has been done in the context of the MICCAI WMH Challenge<sup>5</sup>. The aim was to provide a fully automated pipeline for the segmentation of White Matter Hyperintensities (WMH) of vascular origin. WMH are the consequences of small vessel diseases and are visible on brain MR images [24]. Small vessel

---

<sup>5</sup> <http://wmh.isi.uu.nl>

| Hospital           | Scanner              | Number of training images | Number of test images |
|--------------------|----------------------|---------------------------|-----------------------|
| UMC Utrecht        | 3T Philips Achieva   | 20                        | 30                    |
| NUHS Singapore     | 3T Siemens TrioTim   | 20                        | 30                    |
| VU Amsterdam (AMS) | 3T GE Signa HDxt     | 20                        | 30                    |
|                    | 3T Philips Ingenuity | 0                         | 10                    |
|                    | 1.5T GE Signa HDxt   | 0                         | 10                    |

**Table 1.** Overview of the challenge database.

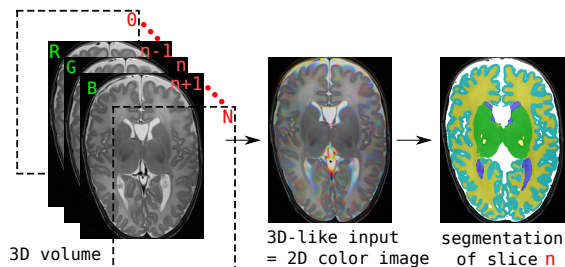


**Fig. 1.** Illustration of 3D-like color image and associated segmentation used in [25].

diseases are involved in cerebrovascular diseases and are a cause of cognitive decline and functional loss during ageing [16]. Studies of WMH parameters (volume, shape, etc.) can hence be a key for diagnosis and follow-up for patients under treatment for dementia and neurodegenerative diseases.

The visual analysis of images to detect WMH is a difficult process and automated methods could helpfully assist diagnosis [1]. However, the evaluation and comparison of automated WMH segmentation techniques remain difficult because of the diversity of datasets and evaluation criteria [1]. The aim of the MICCAI WMH Challenge was to compare automated WMH segmentation techniques. This comparison yields a ranking of the techniques applied on data acquired from different scanner platforms (different origins, different resolutions, etc). Data used during the challenge originated from three hospitals and five different scanners as shown in Tab. 1. A training set of 60 scans was provided by the organizer and the testing set of 110 scans remained secret.

## 1.2 Related Work

WMH segmentation has always been challenging, and it appears to be really complicated to obtain a reliable fully automated method [1, 4]. Indeed, a Dice similarity coefficient will be considered as good if it is higher than 0.7 [1]. The problem of WMH segmentation can be considered with several approaches. The FLAIR modality seems to be one of the best for this kind of segmentation: it is possible to segment the hyperintensities with an optimal FLAIR intensity threshold based on the analysis of histograms as described by Jack et al. [7].

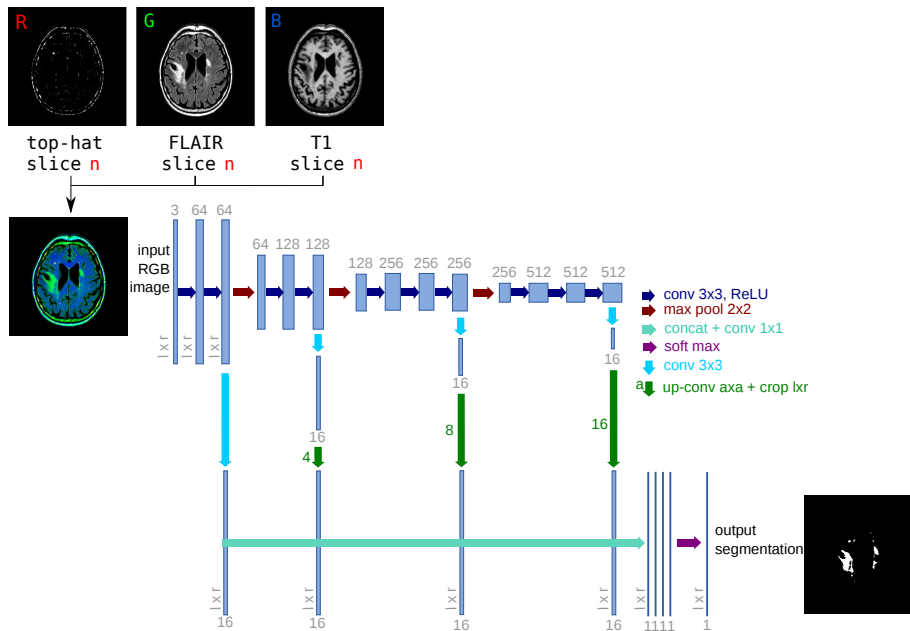


**Fig. 2.** Architecture of the proposed network. We fine tune it and combine linearly fine to coarse feature maps of the pre-trained VGG network [22]. Note that each color image (**Input**) is built from the slice  $n$  of the T1 and FLAIR sequences, and from a pre-processing result.

Some methods rely on random Markov fields, either using FLAIR [9] or some other modality [21]. In [15], morphological operators and max-tree representations are used to segment the WMH in newborn T2 brain images, but this method is not fully automated. As machine learning really improved the results of some segmentation tasks, some new methods emerged using supervised machine learning procedures or unsupervised approaches. In [5] WMH segmentation is performed using CNN with anatomical location information, and in [6] using transfer learning with a domain adaptation and patches, reaching a Dice score of 0.76. The authors suggested the idea to replace their CNN network with a FCN one, for example U-Net [17]. In a previous work published in the International Conference on Image Processing (ICIP) in 2017 [25], 3D brain MR volumes were segmented using fully convolutional network (FCN) and transfer learning. The network used for transfer learning is VGG (Visual Geometry Group) [22], pre-trained on the ImageNet dataset. It takes as input a 2D color image that is here a *3D-like* image, composed of 3 consecutive slices of the 3D volume (see Fig. 1). This method uses only one modality, and reaches good results for brain segmentation.

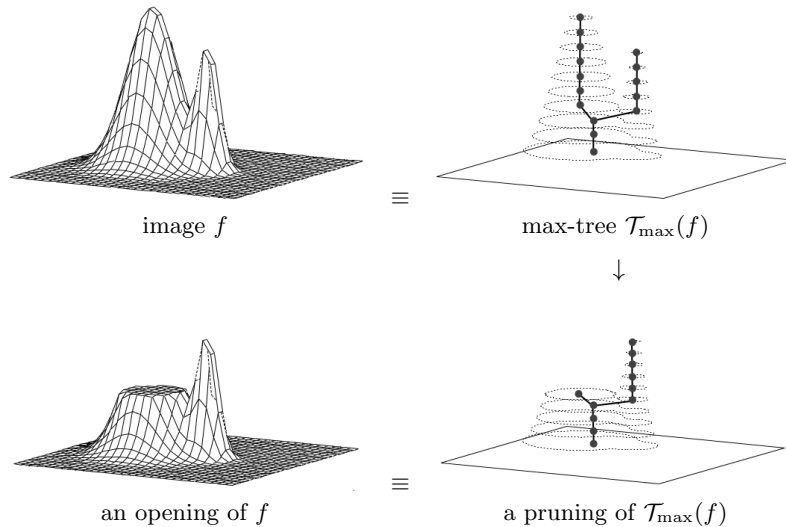


**Fig. 3.** A morphological connected operator (here an opening) based on a tree-based image representation.

For this challenge, we extended this previous work on brain MRI segmentation [25], leveraging the power of a fully convolutional network pre-trained on a large dataset and later fine-tuned on the training set of the challenge. The main contributions include:

1. a preprocessing technique based on mathematical morphology which enhances small lesions to improve their segmentation;
2. a merging technique which enables the input of several modalities (T1, FLAIR and custom preprocessing) in the segmentation chain for each slice.

An overview of the proposed method is given in Fig. 2. The method is fully automatic, and uses both T1 and FLAIR sequences. The details of the whole pipeline are given hereafter. This method is really fast as about 10 seconds are needed to process a complete scan volume, and also efficient: we reached the 6th place during the MICCAI WMH Challenge.

## 2 Method Description

### 2.1 Forewords on Mathematical Morphology

Whereas the most popular operators of mathematical morphology (MM) rely on structuring elements, the class of “connected operators” does not necessarily [11, 20]. This class is very interesting because those operators do not shift object contours (they cannot create some new contours, they just suppress some existing ones). Some connected operators can be easily defined from some tree-based representations of a gray-level image [8, 18, 19]; such image representations

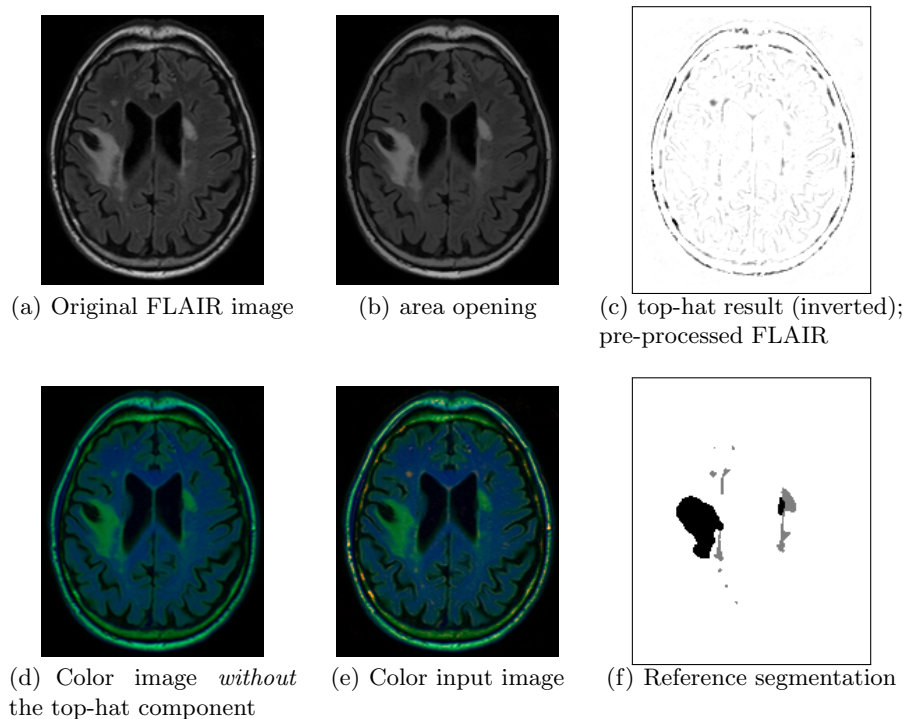


**Fig. 4.** Illustration of the top-hat procedure.

express the inclusion of the connected components obtained by thresholding the image. Note that computing, storing, and processing such a component tree is very efficient [2, 14]. In the following, we rely on the *max-tree* representation, denoted by  $\mathcal{T}_{\max}$ , obtained by upper thresholding. Such a tree is displayed in Fig. 3 (top right). If we prune this tree, such as in Fig. 3 (bottom right), we can reconstruct the function depicted in Fig. 3 (bottom left). In the following, we filter out any component of the max-tree which size (or area, i.e., number of pixels) is below a threshold  $N$ , which leads to an *area opening* [23]. In all our experiments, we set  $N$  to 25 pixels.

In Fig. 4(b), such an operator was applied on the image of Fig. 4(a). In this result, some small bright components are removed, without the rest of the image being modified (it is a connected operator); let us also note that this operator has the ability to filter out low-contrasted objects in the same way as it does with high-contrasted ones. The removed components correspond to small spots of white matter intensities. The residue of this filtering step, i.e., the result minus the input, is called an *area top-hat*; it is depicted in Fig. 4(c).

## 2.2 Pre-Processing

We use the bias field corrected FLAIR image and the bias field corrected T1 image aligned with FLAIR. The main issue with WMH segmentation is the segmentation of small lesions. An idea to help the network find the lesions is to enhance them.

We first perform a requantization of voxel intensity values on 8 bits. The FLAIR slices are filtered using a morphological operator (an area opening), so that small lesions are filtered out, and we compute the residue (difference between the original FLAIR image and the filtered one); in this final image, called “pre-processed FLAIR” in the following and illustrated in Fig. 4(c), small lesions are particularly visible and large ones do not appear.

## 2.3 Deep FCN for WMH Segmentation

Fully convolutional network (FCN) and transfer learning have proved their efficiency for natural image segmentation [12]. In a previous paper [25], we proposed to rely on this method to segment 3D brain MR images, although those images are very different from natural images. As it was a success, we adapted it to WMH segmentation. We rely on the 16 layers VGG network [22], which was pre-trained on millions of natural images of ImageNet for image classification [10]. For our application, we keep only the 4 stages of convolutional parts called “*base network*” and discard the fully connected layers at the end of VGG network. This base network is mainly composed of convolutional layers:  $z_i = w_i \times x + b_i$ , Rectified Linear Unit (ReLU) layers for non linear activation function:  $f(z_i) = \max(0, z_i)$ , and max pooling layers between two successive stages, where  $x$  is the input of each convolutional layer,  $w_i$  is the convolution parameter, and  $b_i$  is the bias term. The three max pooling layers divide the base network into four stages of fine to coarse feature maps. Inspired by the work in [12, 13], we add specialized convolutional layers (with a  $3 \times 3$  kernel size) with  $K$  (e.g.  $K = 16$ ) feature maps after the convolutional layers at the end of each stage. All the specialized layers are then rescaled to the original image size, and concatenated together. We add a last convolutional layer with kernel size  $1 \times 1$  at the end. This last layer combines linearly the fine to coarse feature maps in the concatenated specialized layers, and provides the final segmentation result. The proposed network architecture is schematized in Fig. 2.

The architecture described above is very similar to the one used in [13] for retinal image analysis, where the retinal images are already 2D color images. For our application, the question amounts to how to prepare appropriate inputs given that a brain MR image is a 3D volume. To get RGB input images, we propose to use 2D slices from different modalities. Precisely, to form an input artificial color image for the pre-trained network to segment the  $n^{\text{th}}$  slice, we use the slice  $n$  of FLAIR, of the T1 and of the pre-processed FLAIR as the three different color channels of a 2D color image. The green, blue and red channels thus carry different information; note that the match “particular information / chosen channel” does not matter for the network at end, except that this match

has to remain always the same in the learning and testing stages. This process is depicted in Fig. 2 (left). Each 2D color image thus forms a representation of a part (a slice of FLAIR and T1) of the MR volume. Using such a 2D representation avoids the expensive computational and memory requirements of fully 3D FCN.

For the training phase, we use the multinomial logistic loss function for a one-of-many classification task, passing real-valued predictions through a soft-max to get a probability distribution over classes. During training, we use the classical data augmentation strategy by scaling and rotating. Each channel of the training images is then centered (we subtract 127 to values to ensure input value are within the  $[-127, 127]$  range). We fine tune the network for the first 50k iterations using a learning rate of  $10^{-8}$ , and the last 100k with a smaller learning rate of  $10^{-9}$ . We rely on stochastic gradient descent to minimize the loss function with a momentum of 0.99 for the first 50k iterations and 0.999 for the next 100k, and a weight decay of 0.0005. The loss function is averaged over 20 images.

At test time, after having pre-processed the 3D volume (requantization), we prepare the set of 2D color images. Then we subtract 127 for each channel, and pass every image through the network.

We run the train and test phases on a GPU card: NVIDIA GeForce GTX 1080 Ti, having 11Go. The training phase lasts 4 hours while the testing one lasts less than 10 seconds per volume. The 4 hours of the learning remains reasonable, and the network can be learned again if scans from new machines are provided. It could be useful, especially if the new scans are different (resolution, contrast, etc.).

The output of the network for one slice during the inference phase is a 2D segmented slice. After processing all the slices of the volume, all the segmented slices are stacked to recover a 3D volume with the same shape as the initial volume, and containing only the segmented lesions.

Last, let us remark that, in the case of small lesions, the use of multi-modality can be an important key. Indeed, the small lesions are not present on a lot of slices, thus limiting the interest of 3D representations. The use of combination of T1 and FLAIR images for one slice gives more information for lesion detection. As the proportion of small lesions is small compared to the total number of pixels, every information that can be discriminant for lesion detection is important.

### 3 Experiments and Results

This section presents the experiments and results obtained, during the development of our method first (using the training dataset), and then the results of the challenge. The metrics used to evaluate the results are:

- Dice Similarity Coefficient,
- Hausdorff distance (modified, 95th percentile, in mm) [3],
- Average volume difference (in percentage),
- Sensitivity for individual lesions, or recall (in percentage),

| Type            | Dice $\uparrow$ | AVD $\downarrow$ | Lesion Detection $\uparrow$ | F1 score $\uparrow$ |
|-----------------|-----------------|------------------|-----------------------------|---------------------|
| 3D-like         | 0.72            | 23.90            | 0.38                        | 0.46                |
| 2D w/o top-hat  | 0.72            | 28.24            | 0.39                        | 0.48                |
| 2D with top-hat | 0.75            | 22.63            | 0.61                        | 0.63                |

**Table 2.** Quantitative comparison of the influence of the top-hat on the pre-competition dataset. We submitted the 2D with top-hat method for the challenge. In this table and in the following ones,  $\uparrow$  (resp.  $\downarrow$ ) means that a higher (resp. lower) value is better.

| Origin                    | Dice $\uparrow$ | H95 $\downarrow$ | AVD $\downarrow$ | Recall $\uparrow$ | F1 $\uparrow$ |
|---------------------------|-----------------|------------------|------------------|-------------------|---------------|
| UMC Utrecht               | 0.74            | 11.22            | 19.07            | 0.70              | 0.66          |
| NUHS Singapore            | 0.77            | 8.28             | 17.64            | 0.61              | 0.68          |
| AMS GE 3T                 | 0.75            | 6.75             | 21.91            | 0.62              | 0.71          |
| AMS GE 1.5T               | 0.73            | 10.94            | 16.66            | 0.60              | 0.71          |
| AMS Philips 3T            | 0.50            | 70.27            | 46.33            | 0.57              | 0.53          |
| Weighted average          | 0.73            | 14.54            | 21.71            | 0.63              | 0.67          |
| Rank [0...1] $\downarrow$ | 0.122           | 0.180            | 0.004            | 0.352             | 0.159         |

**Table 3.** Results of our method on the challenge dataset. The five first lines are the results for each metric of each pool of data. The sixth line is the weighted average of each metric. The last line corresponds to the rank for each metric.

- F1-score for individual lesions:  $2PR/(P+R)$ , where  $P$  and  $R$  are respectively the precision and the recall.

### 3.1 Development Phase

In this part, we used the 60 scans from the training set of the challenge to validate and tune our approach. Those scans were acquired in three hospitals using three scanners from different vendors (see Tab. 1).

*Training.* We trained our model on 30 scans (10 from each hospital), randomly chosen. The model was trained using the parameters described in the previous section.

*Testing.* We tested on the 30 remaining scans. We measured 4 parameters using the code provided by the organizers: the dice coefficient, the average volume distance (AVD), the sensitivity for individual lesion detection and the F1-score for individual lesions. The results are shown in Tab. 2, line 3.

An illustration of our segmentation results, with a qualitative comparison to the reference segmentation, can be found in Fig. 5. False negatives and false positives are very reduced.

| TEAM         | RANK ↓        | DSC ↑       | H95 ↓        | AVD ↓        | RECALL ↑    | F1 ↑        |
|--------------|---------------|-------------|--------------|--------------|-------------|-------------|
| nlp_logix    | 0.0485        | 0.77        | 7.16         | 18.37        | 0.73        | 0.78        |
| k2           | 0.1368        | 0.77        | 9.79         | 19.08        | 0.59        | 0.70        |
| ipmi-bern    | 0.2498        | 0.69        | 9.72         | 19.92        | 0.44        | 0.57        |
| misp         | 0.1659        | 0.72        | 14.88        | 21.36        | 0.63        | 0.68        |
| <b>lrde</b>  | <b>0.1635</b> | <b>0.73</b> | <b>14.54</b> | <b>21.71</b> | <b>0.63</b> | <b>0.67</b> |
| cian         | 0.0366        | 0.78        | 6.82         | 21.72        | 0.83        | 0.70        |
| sysu_media   | 0.0076        | 0.80        | 6.30         | 21.88        | 0.84        | 0.76        |
| achilles     | 0.2962        | 0.63        | 11.82        | 24.41        | 0.45        | 0.52        |
| nic-vicorob  | 0.0735        | 0.77        | 8.28         | 28.54        | 0.75        | 0.71        |
| tig          | 0.3858        | 0.60        | 17.86        | 34.34        | 0.38        | 0.42        |
| scan         | 0.2762        | 0.63        | 14.34        | 34.67        | 0.55        | 0.51        |
| knight       | 0.4159        | 0.70        | 17.03        | 39.99        | 0.25        | 0.35        |
| skkumedneuro | 0.3492        | 0.58        | 19.02        | 58.54        | 0.47        | 0.51        |
| tignet       | 0.3802        | 0.59        | 21.58        | 86.22        | 0.46        | 0.45        |
| nist         | 0.4747        | 0.53        | 15.91        | 109.98       | 0.37        | 0.25        |
| text_class   | 0.5725        | 0.50        | 28.23        | 146.64       | 0.27        | 0.29        |
| nih_cidi     | 0.2697        | 0.68        | 12.82        | 196.38       | 0.59        | 0.54        |
| upc_dlmi     | 0.4337        | 0.53        | 27.01        | 208.49       | 0.57        | 0.42        |
| neuro.ml     | 0.5960        | 0.51        | 37.36        | 614.05       | 0.71        | 0.21        |
| hadi         | 0.8886        | 0.23        | 52.02        | 828.61       | 0.58        | 0.11        |

**Table 4.** Competition results, sorted with respect to the AVD metric.

*Validation of the top-hat 2D choice.* To evaluate the influence of the top-hat and the 2D input on our results, we trained and tested with and without the top-hat on 2D images (the last channel was replaced by the same slice from T1) and we tested the 3D-like approach from our previous work [25]. Results are shown in Tab. 2. The results of the 3D-like approach and of the 2D approach *without* top-hat are quite similar. The lesion detection is a little bit better for the 2D combination, but this is not significant. The 3D information is hence not relevant for this application. The 2D approach including the top hat image slightly improved the Dice and the AVD, but the best improvement is for the lesion detection. On this dataset, the measurement of the sensitivity for individual lesion raised from 0.38% or 0.39% to 0.61% thanks to the 2D top-hat procedure. The small lesions enhancement indeed helped the detection of lesions.

### 3.2 Challenge Results

The testing dataset of the MICCAI WMH Challenge remained secret. It was composed of 110 scans of patients from three hospitals and five different scanners from three vendors (see Tab. 1).

The metrics used for the evaluation are the five metrics described at the beginning of this section. The rank is included between 0 (best result) and 1 (worst result). It is computed by the organizers of the challenge as follows: the teams are sorted from best to worst for each metric. The best team will be ranked 0 and the worst team 1. The other teams are ranked between 0 and 1 relative to their performance within the range of that metric. The final rank is the average of the 5 metric ranks. Tab. 3 shows the results of our method for the challenge.

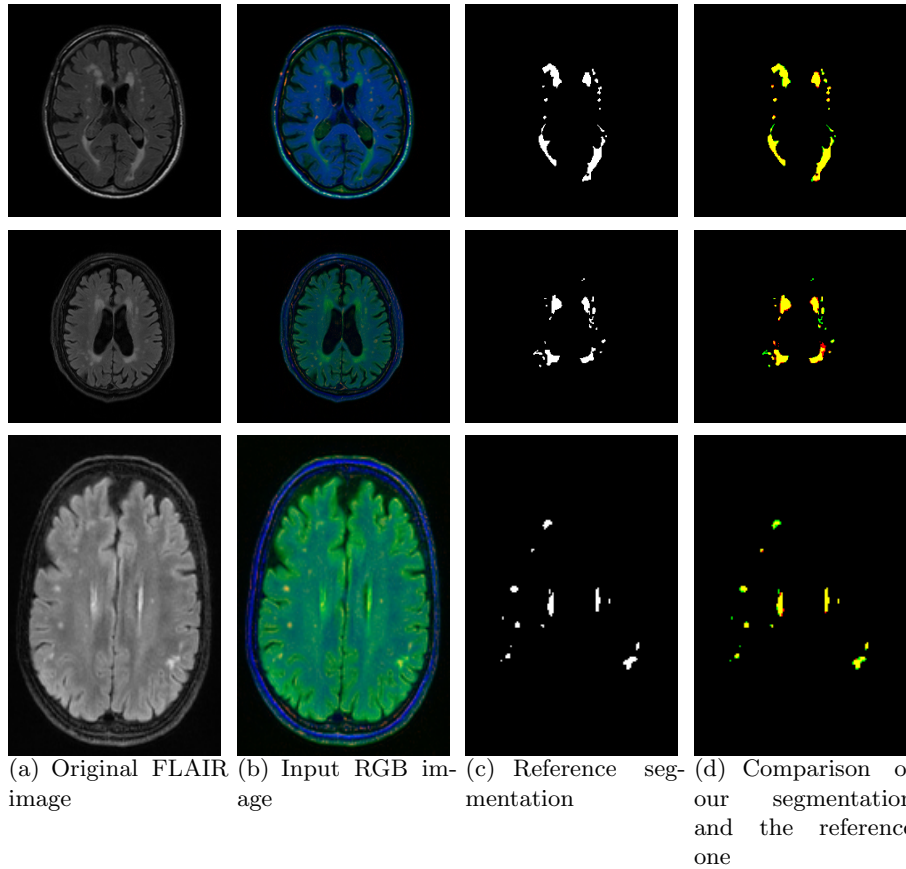


**Fig. 5.** Example of results on each database. Note that the input images are different as they come from different hospitals. From top to bottom: Utrecht, Singapore, and Amsterdam. The intersection between the reference segmentation and our result is depicted in yellow; the green pixels (false negatives) are in the reference segmentation but not in our segmentation; the red ones (false positives) are in our segmentation but not in the reference one.

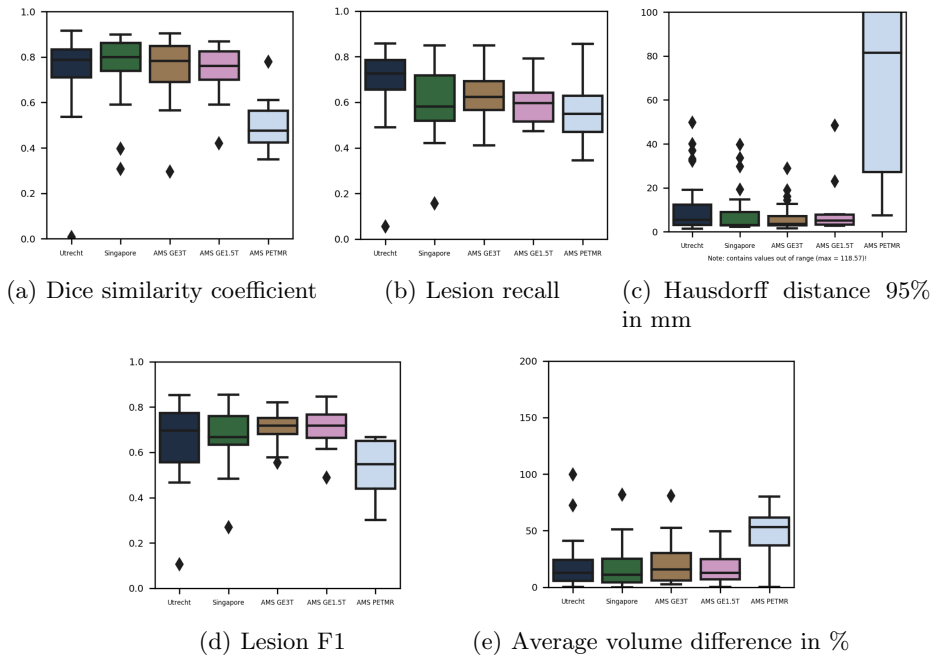


**Fig. 6.** Box plot for each metric depending on the origin of the scans; UMC Utrecht in dark blue, NUHS Singapore in green, and VU Amsterdam (AMS): 3T GE Signa HDxt in brown, 3T Philips Ingenuity in pink, and 1.5T GE Signa HDxt in light blue.

Our best performance is for the AVD where we have a really good rank as shown in Tab. 3 and Tab. 4, while our worst score is for the lesion detection. Based on these measurements, we can conclude that our method still misses some lesions but that the ones it detects are close to the reference segmentation. We were ranked 0.164 on the overall average and reached the 6<sup>th</sup> place of the challenge. The top methods of the challenge also use deep learning for the segmentation. They mainly use patches of images instead of whole images. About the architecture used, it is interesting to notice that the winner of this challenge uses a U-Net architecture with pre-processing and post-processing steps.

The analysis of the results against each data source reveals that our method performs poorly on data acquired with the Philips scanner, for which no training data were available and test images remained secret, preventing us from investigating further. We can also note that while no training data were available for the GE 1.5T, our method still performs well on such data. The box plots (Fig. 6) show the inhomogeneities of these results. Despite this, our method appears quite stable among the different acquisition devices.

## 4 Conclusion

In the context of the MICCAI WMH Challenge, we developed a fast, robust and automated method that segments white matter hyperintensities (WMH) in 3D brain MR images. It is an extension of a method we proposed for brain MRI segmentation. It uses fully convolutional network (FCN) and transfer learning to segment the lesions. It takes as input 2D color images (3 channels), corresponding to a slice of a 3D volume. The two first channels are composed of a combination of FLAIR and T1 slices. To improve the detection of the lesions, the last channel is a modified FLAIR slice where the small hyperintensities are enhanced by a top-hat procedure. The FCN is the VGG network for natural image classification, pre-trained on ImageNet database. We fine tuned it on the training dataset of the challenge. When all slices are processed, the results are stacked to reconstruct the resulting 3D segmented volume. During the development phase, we validated the benefits of the 2D pre-processed images with small lesions enhancement over the 2D images containing only T1 and FLAIR slices, and also over a 3D-like image as in [25]. With such a technique, the complete segmentation of WMH on a 3D brain volume takes about 10 seconds. During the challenge, the organizers ran our method on their database composed of 5 different sets. Our results are quite stable over acquisition methods except for the Philips scanner, thus exhibiting the reliability of our method. Finally, we achieved a top score on the AVD metric with a rank of 0.004 (best is 0, worst is 1) for an AVD value of 21.71. Our overall score is 0.164 (average of the 5 metrics used for the challenge), leading us to the 6th place. With our method, we could consider other applications for other purposes such as the TUPAC16 MICCAI Grand Challenge (Tumor Proliferation Assessment Challenge 2016) which aims to predict the tumor proliferation score for breast cancer, or the Multimodal Brain Tumor Segmentation Challenge (BraTS) which focuses on the prediction of patient overall survival from the study of brain lesions.

**Acknowledgments** The authors want to thank the organizers of the White Matter Hyperintensities Segmentation Challenge at MICCAI 2017, and the reviewers for their valuable comments.

## References

1. Caligiuri, M.E., Perrotta, P., Augimeri, A., Rocca, F., Quattrone, A., Cherubini, A.: Automatic detection of white matter hyperintensities in healthy aging and pathology using magnetic resonance imaging: A review. *Neuroinformatics* 13(3), 261–276 (2015)
2. Carlinet, E., Géraud, T.: A comparative review of component tree computation algorithms. *IEEE Transactions on Image Processing* 23(9), 3885–3895 (2014)
3. Dubuisson, M.P., Jain, A.K.: A modified Hausdorff distance for object matching. In: *Proceedings of the 12th International Conference on Pattern Recognition*. vol. 1, pp. 566–568. IEEE (1994)

4. García-Lorenzo, D., Francis, S., Narayanan, S., Arnold, D.L., Collins, D.L.: Review of automatic segmentation methods of multiple sclerosis white matter lesions on conventional magnetic resonance imaging. *Medical Image Analysis* 17(1), 1–18 (2013)
5. Ghafoorian, M., Karssemeijer, N., Heskes, T., van Uden, I.W., Sanchez, C.I., Litjens, G., de Leeuw, F.E., van Ginneken, B., Marchiori, E., Platel, B.: Location sensitive deep convolutional neural networks for segmentation of white matter hyperintensities. *Scientific Reports* 7(5110) (2017)
6. Ghafoorian, M., Mehrtash, A., Kapur, T., Karssemeijer, N., Marchiori, E., Pesteie, M., Guttman, C.R., de Leeuw, F.E., Tempny, C.M., van Ginneken, B., Fedorov, A., Abolmaesumi, P., Platel, B., Wells III, W.M.: Transfer learning for domain adaptation in MRI: Application in brain lesion segmentation. In: *Proceedings of International Conference on Medical Image Computing and Computer Assisted Intervention (MICCAI), Part III. Lecture Notes in Computer Science*, vol. 10435, pp. 516–524. Springer (2017)
7. Jack, C.R., O’Brien, P.C., Rettman, D.W., Shiung, M.M., Xu, Y., Muthupillai, R., Manduca, A., Avula, R., Erickson, B.J.: FLAIR histogram segmentation for measurement of leukoaraiosis volume. *Journal of Magnetic Resonance Imaging* 14(6), 668–676 (2001)
8. Jones, R.: Component trees for image filtering and segmentation. In: Coyle, E. (ed.) *Proceedings of the IEEE Workshop on Nonlinear Signal and Image Processing*. Mackinac Island (1997)
9. Khayati, R., Vafadust, M., Towhidkhan, F., Nabavi, M.: Fully automatic segmentation of multiple sclerosis lesions in brain MR FLAIR images using adaptive mixtures method and Markov random field model. *Computers in Biology and Medicine* 38(3), 379–390 (2008)
10. Krizhevsky, A., Sutskever, I., Hinton, G.E.: Imagenet classification with deep convolutional neural networks. In: *Advances in neural information processing systems*. pp. 1097–1105 (2012)
11. Lazzara, G., Géraud, T., Levillain, R.: Planting, growing and pruning trees: Connected filters applied to document image analysis. In: *Proceedings of the 11th IAPR International Workshop on Document Analysis Systems (DAS)*. pp. 36–40. Tours, France (2014)
12. Long, J., Shelhamer, E., Darrell, T.: Fully convolutional networks for semantic segmentation. In: *Proceedings of IEEE International Conference on Computer Vision and Pattern Recognition*. pp. 3431–3440 (2015)
13. Maninis, K.K., Pont-Tuset, J., Arbeláez, P., Gool, L.V.: Deep retinal image understanding. In: *Proceedings of International Conference on Medical Image Computing and Computer Assisted Intervention (MICCAI), Part II. Lecture Notes in Computer Science*, vol. 9901, pp. 140–148. Springer (2016)
14. Meijster, A., Wilkinson, M.H.F.: A comparison of algorithms for connected set openings and closings. *IEEE Transaction on Pattern Analysis and Machine Intelligence* 24(4), 484–494 (2002)
15. Morel, B., Xu, Y., Virzi, A., Géraud, T., Adamsbaum, C., Bloch, I.: A challenging issue: Detection of white matter hyperintensities on neonatal brain MRI. In: *Proceedings of the Annual International Conference of the IEEE Engineering in Medicine and Biology Society (EMBC)*. pp. 93–96 (2016)
16. Pantoni, L.: Cerebral small vessel disease: From pathogenesis and clinical characteristics to therapeutic challenges. *The Lancet Neurology* 9(7), 689–701 (2010)

17. Ronneberger, O., Fischer, P., Brox, T.: U-net: Convolutional networks for biomedical image segmentation. In: Proceedings of International Conference on Medical Image Computing and Computer Assisted Intervention (MICCAI), Part III. Lecture Notes in Computer Science, vol. 9351, pp. 234–241. Springer (2015)
18. Salembier, P., Oliveras, A., Garrido, L.: Antiextensive connected operators for image and sequence processing. *IEEE Transactions on Image Processing* 7(4), 555–570 (1998)
19. Salembier, P., Serra, J.: Flat zones filtering, connected operators and filters by reconstruction. *IEEE Transaction on Image Processing* 3(8), 1153–1160 (1995)
20. Salembier, P., Wilkinson, M.H.: Connected operators. *IEEE Signal Processing Magazine* 26(6), 136–157 (2009)
21. Schwarz, C., Fletcher, E., DeCarli, C., Carmichael, O.: Fully-automated white matter hyperintensity detection with anatomical prior knowledge and without FLAIR. *Information Processing in Medical Imaging* 21, 239–251 (2009)
22. Simonyan, K., Zisserman, A.: Very deep convolutional networks for large-scale image recognition. *CoRR* abs/1409.1556 (2014)
23. Vincent, L.: Grayscale area openings and closings, their efficient implementation and applications. In: Proc. of the EURASIP 1st Workshop on Mathematical Morphology and its Applications to Signal Processing. pp. 22–27. Barcelona, Spain (May 1993)
24. Wardlaw, J.M., Smith, E.E., Biessels, G.J., Cordonnier, C., Fazekas, F., Frayne, R., Lindley, R.I., O’Brien, J.T., Barkhof, F., Benavente, O.R., et al.: Neuroimaging standards for research into small vessel disease and its contribution to ageing and neurodegeneration. *The Lancet Neurology* 12(8), 822–838 (2013)
25. Xu, Y., Géraud, T., Bloch, I.: From neonatal to adult brain MR image segmentation in a few seconds using 3D-like fully convolutional network and transfer learning. In: Proceedings of the 23rd IEEE International Conference on Image Processing (ICIP). pp. 4417–4421. Beijing, China (September 2017), <http://www.lrde.epita.fr/~theo/papers/geraud.2017.icip.pdf>